CDF/DOC/JET/PUBLIC/8928

Measurement of the Inclusive Jet Cross Section Using the Midpoint Algorithm in Run II at CDF

The CDF Collaboration
URL http://www-cdf.fnal.gov
(Dated: July 24, 2007)

A measurement is presented of the inclusive jet cross section using the Midpoint jet clustering algorithm in the rapidity region of $|y| < 2.1$. The results are consistent with NLO pQCD predictions using the CTEQ6.1 parton density functions.

Preliminary Results for Summer 2007 Conferences

I. INTRODUCTION

The measurement of the differential inclusive jet cross section at CDF reaches the highest momentum transfers ever directly studied in collider experiments, and thus it is potentially sensitive to new physics such as quark substructure [1, 2]. Studying the highest energy events at the Tevatron is equivalent to probing distances on the order of 10^{-19} m. The inclusive jet cross section measurement also provides a fundamental test of predictions of perturbative QCD (pQCD) [3, 4] over eight orders of magnitude in cross section. The measurement spans 600 GeV/c in jet transverse momentum (p_T), and it can therefore be used to observe the running of α_s in a single measurement. Perhaps most importantly, the inclusive jet measurement can be used to constrain the (anti)proton PDF which in turn improves the theoretical predictions in all physics channels for experiments at the Tevatron and future experiments at the LHC.

Because the inclusive jet measurement in the forward region (large y [29]) probes a kinematic region which is not expected to be sensitive to new physics, it leads to a powerful constraint on the gluon PDF. This is important because the gluon PDF is very poorly constrained at high x [5]. The gluon PDF is the dominant source of theoretical uncertainty in the inclusive jet cross section and many other processes at hadron colliders.

In Run 1, CDF measured the inclusive jet cross section in the central region of the detector ($0.1 < |\eta| < 0.7$) using a cone jet clustering algorithm [6]. A new inclusive jet cross section measurement in the central region ($0.1 < |y| < 0.7$) using the cone-based Midpoint jet algorithm in Run 2 has been published recently by CDF [7]. The Midpoint jet finding algorithm is described in detail elsewhere [8, 9]. CDF also recently published inclusive jet measurements in the central region [10] and including the forward region [11] for jets clustered by the k_T algorithm. This note is an update of the previous analysis using the Midpoint algorithm with more than twice the integrated luminosity and including the forward rapidity region ($|y| < 2.1$) [30].

The rest of this document proceeds as follows: Section II describes the CDF detector components most relevant to this analysis. In section III details of the data sample included in the analysis are discussed. Section IV explains the corrections used to correct the CDF data to the hadron level so that it may be compared directly with the predictions of pQCD. The Monte Carlo (MC) and CDF detector simulation that are used to derive these corrections are also discussed in this section. Systematic uncertainties on the final cross section measurement are discussed in section V. Finally, in sections VI and VII the corrected results are presented and compared with the pQCD predictions.

II. THE CDF DETECTOR

The CDF detector is described in detail in [12, 13]. Here, those components that are crucial to this measurement are briefly described. The central detector consists of a silicon vertex detector inside a cylindrical drift chamber. Surrounding the tracking detectors is a superconducting solenoid which provides a 1.4 T magnetic field. Outside the solenoid is the central calorimeter divided into electromagnetic (CEM) and hadronic (CHA) sections. The central calorimeter consists of 48 modules, segmented into towers of granularity $\Delta\eta \times \Delta\phi \approx 0.1 \times 0.26$, and covers a pseudo-rapidity range up to 1.1. The CEM is a lead-scintillator calorimeter with a depth of about 18 radiation lengths; the CHA is an iron-scintillator calorimeter with a depth of approximately 4.7 interaction lengths. The energy resolution of the CEM for electrons is $\sigma(E_T)/E_T = 13.5\ \%/\sqrt{E_T(\mathrm{GeV})} \oplus 2\ \%$ while the average energy resolution of the CHA for charged pions is $\sigma(E_T)/E_T = 50\ \%/\sqrt{E_T(\mathrm{GeV})} \oplus 3\ \%$.

The forward region, $1.1 < |\eta| < 3.6$, is covered by the “Plug Calorimeters” consisting of lead-scintillator for the electromagnetic section and iron-scintillator for the hadronic section. The PEM and PHA are identically segmented into 480 towers of size which varies with η ($\Delta\eta \times \Delta\phi \approx 0.1 \times 0.13$ at $|\eta| < 1.8$ and increases to $\Delta\eta \times \Delta\phi \approx 0.6 \times 0.26$ at $|\eta| = 3.6$). The energy resolution of the PEM for electrons is $\sigma(E_T)/E_T = 16\ \%/\sqrt{E_T(\mathrm{GeV})} \oplus 1\ \%$ while the average energy resolution of the PHA for charged pions is $\sigma(E_T)/E_T = 80\ \%\sqrt{E_T(\mathrm{GeV})} \oplus 5\ \%$. The region between the central and forward calorimeters, $0.7 < |\eta| < 1.3$, is covered by an iron-scintillator hadron calorimeter (WHA) with similar segmentation to the central calorimeter. The WHA has a depth of approximately 4.5 interaction lengths, and a resolution for charged pions of $\sigma(E_T)E_T = 75\ \%\sqrt{E_T(\mathrm{GeV})} \oplus 3\ \%$.

III. DATA SAMPLE & EVENT SELECTION

This analysis includes data taken from February 2002 until February 2006 and corresponds to an integrated luminosity of 1.13 fb^{-1}. The jet data used in this analysis were collected using four paths in the CDF three-level trigger system [14]. The four jet trigger paths used in this analysis are summarized in table I. The level 1 trigger requires a calorimeter trigger tower to have either $E_T > 5$, $E_T > 10$, or $E_T > 20$ GeV. At level 2, the calorimeter towers are clustered using a nearest neighbor algorithm. Four trigger paths with cluster $E_T > 15$, 40, 60, and 90 GeV are used.

TABLE I: Summary of the jet triggers used in this analysis. For each dataset, the E_T threshold on the trigger towers at level-1, calorimeter clusters at level-2 and jets clustered at level-3, and the corresponding prescales are shown. When multiple numbers are shown in a single column, it means the prescale factor or the E_T threshold changed during the data taking period studied.

Dataset	level-1		level-2		level-3	
	E_T	Prescale	E_T	Prescale	E_T	Prescale
Jet20	5	20,50	15	12,25	20	1
Jet50	5	20,50	40	1,5	50	1
Jet70	10	1	60	8	70	1
Jet100	10,20	1	90	1	100	1

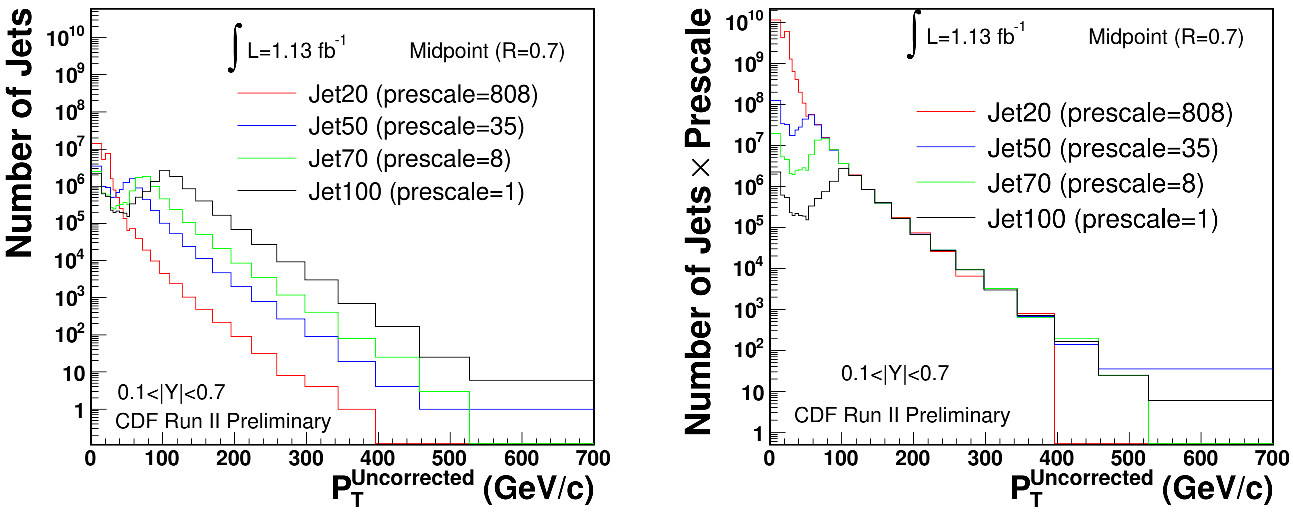

FIG. 1: Jet yield distributions as a function of p_T in the central region $(0.1 < |y| < 0.7)$ before (left) and after (right) correcting for trigger prescales.

Events in these paths are required to pass jet $E_T > 20$, 50, 70, and 100 GeV thresholds at level 3, where the clustering is performed using a cone algorithm with a cone radius $R_{cone} = 0.7$.

Cosmic ray and other backgrounds are removed by applying a missing E_T significance [31] cut. This is a sliding cut based on the highest p_T jet in the event and is defined by:

$$\widetilde{\not{E}_T} < \min(3 + (5/400.) \times p_T^{MAX}, 6); \tag{1}$$

where p_T^{MAX} is the maximum raw jet p_T in the event in unit of GeV/c. The $\widetilde{\not{E}_T}$ cut is about 100 % efficient for low p_T jets and the acceptance decreases to about 90 % for the highest p_T jets used in this analysis. In order to ensure that particles from the $p\bar{p}$ interactions are well measured by the CDF detector, primary vertices are required to have $|Z| < 60$ cm. The acceptance of the Z vertex requirement has been measured from data to be 0.958 ± 0.002.

The jet20, 50 and 70 triggers are prescaled to avoid saturating the bandwidth of the trigger and data acquisition system. The jet70 trigger is prescaled by a constant factor of 8 for all data used in this analysis. The prescale for the jet20 and 50 triggers have changed during the data period considered. The *effective* prescales of the jet20 and 50 triggers for all the data were found to be 808 and 35, respectively. To calculate the effective prescales, the cross section ratio (before prescale correction) of jet50 to jet20 trigger and the ratio of jet70 to jet50 in the region where both trigger samples are efficient were studied. The jet yield distributions as function of p_T in the central region $(0.1 < |y| < 0.7)$ before and after correcting for trigger prescales are shown in figure 1.

The inclusive differential jet cross section is defined as:

$$\frac{d^2\sigma}{dp_T dy} = \frac{1}{\Delta y} \frac{1}{\int \mathcal{L} dt} \frac{N_{jet}/\epsilon}{\Delta p_T}, \tag{2}$$

where N_{jet} is the number of jets in the p_T range Δp_T, ϵ is the $\widetilde{\not{E}_T}$ and vertex cut efficiencies, $\int \mathcal{L} dt$ is the effective integrated luminosity which is corrected for trigger prescales, and Δy is the rapidity interval. A trigger efficiency greater than 99.5 % is required to include the jets collected by a given jet trigger. The inclusive differential jet cross section is split into five jet rapidity regions for this measurement. The regions $|y| < 0.1$, $0.1 < |y| < 0.7$, $0.7 < |y| < 1.1$, $1.1 < |y| < 1.6$, and $1.6 < |y| < 2.1$ were based on detector geometry.

IV. JET CORRECTIONS

The jet energy measured by the calorimeters must be corrected for detector effects, such as calorimeter non-linearity and energy smearing, before comparing experimental measurements with theoretical predictions. Figure 2 describes the jet correction scheme used to obtain results corrected to the hadron [32] or parton level. First, an η-dependent relative correction is applied to the data and MC (the data and MC corrections are slightly different) in order to equalize the response of the CDF calorimeters to jets in y. The equalized jet p_T is then corrected for the pileup effect, *i.e.,* the effect of additional $p\bar{p}$ interactions in the same bunch crossing. Then, the average (absolute) correction is applied to correct on average for the hadron energy that is not measured by the calorimeter. After that, the hadron and calorimeter level jet p_T distributions are compared in Monte Carlo to derive a bin-by-bin correction in order to remove resolution effects (unfolding). After correcting for pileup, absolute scale, and resolution effects the data has been corrected to the hadron level. In order to compare directly with pQCD predictions, the effect of the underlying event (UE) and hadronization needs to be removed from the data. After this final correction, data is corrected to the parton level.

The Monte Carlo simulation used to derive the corrections, and the details of each correction step are described below.

A. Monte Carlo Simulation

The parton shower MC programs PYTHIA 6.2 [15] and HERWIG 6.4 [16] along with the CDF detector simulation are used to derive the various corrections which are applied to the data, and to estimate systematic uncertainties. Structure functions for the proton and anti-proton are taken from CTEQ5L [17]. The CDF detector simulation is based on GEANT3 [18] in which a parametrized shower simulation, GFLASH [19], is used to simulate the energy deposited in the calorimeter [20].

The GFLASH parameters are tuned to test-beam data for electrons and high momentum charged pions and to the *in-situ* collision data for electrons from Z decays and low momentum charged hadrons. However, it is known that the CDF simulation does not describe energy deposition in calorimeters perfectly, especially in the regions corresponding to the plug calorimeters and cracks between calorimeter modules. Since the MC simulation is used to derive various jet corrections to be made on data, differences between the real calorimeter response to jets and the calorimeter simulation need to be well understood. Differences in the relative jet energy response and jet energy resolution between the collision data and MC simulation events were investigated using dijet p_T balancing in dijet events [20] and the *bisector* method [21], respectively.

Comparisons of dijet p_T balance between data and MC show that the relative jet energy scale versus η is different between data and MC and the difference depends on jet p_T at high rapidity ($|y| > 1.1$). For example, the jet energy scale in the plug calorimeter region is higher in MC than in data by ~ 2 % and the difference increases slightly with jet p_T. This difference is accounted for by the relative corrections which are described in detail in section IV B.

The bisector method allows the energy resolution of the CDF detector and the CDF detector simulation to be compared. In the central region ($0.1 < |y| < 0.7$) the detector simulation reproduces the detector jet energy resolution well. In some other y regions it was found that MC slightly underestimates the jet energy resolution in data; to account for these differences, extra smearing is made on jet energies in MC events to match the jet energy resolution between data and MC when the absolute and unfolding corrections are derived. The extra jet energy smearing results in < 6 % changes in cross section in most bins, and still < 15 % in the most extreme cases.

B. Relative Correction

The calorimeter response to jets is not flat in η. The non-uniformity in η arises from cracks between calorimeter modules and also the different responses of the central and plug calorimeters. The relative correction is introduced to make jet energy response flat in η.

The leading two jets in dijet events are expected to balance in p_T in absence of QCD radiation. Therefore, dijet p_T balance in dijet events is a useful tool to study the jet energy response as a function of η and to derive the relative

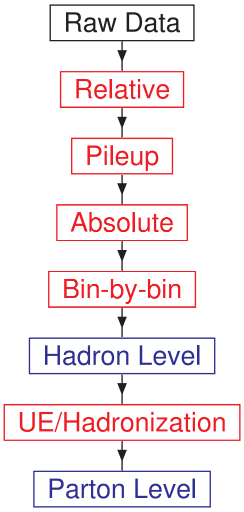

FIG. 2: The flow diagram for the jet corrections used in this analysis is shown in the figure. Correction steps are shown in red, while the hadron level and parton level corrected states are shown in blue. Relative, pileup and average (absolute) corrections are applied directly to the jet p_T before binning.

correction. To determine the η-dependent relative jet energy correction, we define a jet with $0.2 < |\eta| < 0.6$ (where the CDF calorimeter is well understood) as a trigger jet and define the other jet as a probe jet. The p_T balance of these two jets as function of probe jet η provides the relative correction [20].

By making a spline fit to the dijet p_T balance distribution at a given jet p_T, we obtained the η-dependent relative corrections. Since the relative jet energy response is different between data and MC, corrections are derived separately for data and MC. As mentioned earlier, the data-MC difference in the relative jet energy scale depends on jet p_T at $|y| > 1.1$. Therefore, another p_T-dependent correction derived for two highest y regions is applied to the MC to match MC to data at any jet p_T. Due to lack of statistics at high p_T in data, the uncertainty associated with this correction increases with increasing jet p_T.

C. Pileup Correction

Extra $p\bar{p}$ interactions in the same bunch crossing as the interaction which produced jets contribute energy to the jet clustering cone. The number of reconstructed primary vertices is a good estimator of the number of interactions in the same bunch crossing. The correction for the additional $p\bar{p}$ interactions is derived by measuring p_T in a randomly chosen cone as a function of the number of primary vertices in minimum bias events. The p_T in the randomly chosen cone scales linearly with the number of additional vertices in the event, and the pileup correction is derived from the slope of this line.

D. Absolute Correction

As hadrons pass through the CDF calorimeter, all of their energy is not collected. The absolute correction corrects the jet for this average energy loss and is derived by comparing hadron level and calorimeter level jets using PYTHIA and the CDF detector simulation. Hadron level and calorimeter level jets are matched by their position in $y-\phi$ space ($\Delta R = \sqrt{\Delta Y^2 + \Delta\phi^2} \leq 0.7$). The average hadron level jet energy is then studied as a function of the the calorimeter jet energy in each rapidity region. This distribution is fit to a fourth order polynomial and the fit is applied as a correction to the p_T of each jet in the data sample.

E. Unfolding Correction

The next step in correcting the jet p_T distribution to the hadron level is the unfolding correction which removes smearing effects of the calorimeter and accounts for the efficiency of the event selection cuts. The hadron level and calorimeter level (after the absolute correction has been applied) p_T distributions from the PYTHIA MC are compared on a bin-by-bin basis to derive the correction.

After the unfolding correction is applied to the data, the measurement has been corrected to the hadron level. It is now possible to compare the data directly with PYTHIA at the hadron level. In all y regions the PYTHIA p_T distribution falls off faster than the data at high p_T. This could be due to the fact that the PYTHIA samples were generated with the CTEQ5L PDF functions which do not include the enhanced high x gluon distribution that was needed to fit Run 1 CDF inclusive jet data [6]. Regardless of the physics source of the discrepancy, PYTHIA is used to correct the data back to the hadron level and thus the shape of the predicted PYTHIA distributions should be the same as that seen in the data in order to avoid introducing any bias with this correction.

The ratios of data corrected to the hadron level divided by the PYTHIA prediction are fit to polynomials and used to re-weight the PYTHIA p_T distributions to make the shape agree with the data. The unfolding correction factors obtained from the weighted PYTHIA distributions is applied to the data. The change due to the re-weighting of PYTHIA is small (less than 5 %) except for the highest p_T bins where the correction is still less than 20 %.

F. Hadron to Parton Correction

When the absolute and unfolding corrections have been applied to the data, it has been corrected to the hadron level. Before it can be directly compared to pQCD theoretical predictions, the effects of the UE and fragmentation must be removed. The hadron to parton level correction is obtained from comparing PYTHIA-Tune A [33] MC results at the hadron and the parton level to derive a bin-by-bin correction. Tune A has been tuned to fit the underlying event measured at CDF [34]. It is used for all PYTHIA calculations mentioned in this text, but is especially important for the UE correction [22]. The hadron to parton-level correction derived from PYTHIA is shown in figure 3.

V. SYSTEMATIC UNCERTAINTIES

The main sources for systematic uncertainty in the analysis are summarized below.

- Jet energy scale: The systematic uncertainty due to the jet energy scale is dominant in most p_T regions. The uncertainty in the jet energy scale is dominated by the uncertainty in the calorimeter simulation tuning in the central region $0.2 < |\eta| < 0.6$ based on the response to individual particles. This uncertainty is less than 3 % of the jet energy and is expressed in a functional form [20]. The corrected jet p_T in the PYTHIA MC with detector simulation was varied according to this parametrization and the result was compared with the central value. The systematic uncertainty on the cross section measurement varies from 10 % at low p_T up to 90 % at high p_T in some rapidity regions.

- Dijet p_T balance: As discussed above, there is uncertainty on the correction based on the dijet balance in the higher rapidity regions ($|y| > 1.1$) at high p_T due to lack of statistics.

- Unfolding: Difference between PYTHIA and HERWIG is used as the systematic uncertainty on the unfolding correction as they have different fragmentation models. The systematic uncertainty on the measured cross section is taken from the ratio of the unfolding factors obtained from PYTHIA and HERWIG.

- Jet energy resolution: Due to the sharply falling spectrum of the inclusive jet cross section, any imperfection in the jet energy smearing of the detector simulation will affect the derived unfolding correction. The calorimeter level jets in the PYTHIA simulation have been smeared by an extra amount so that the result from the bisector method changes by 10 %. The effect of this extra smearing on the distribution compared with the central measurement is taken as the systematic uncertainty on the cross section due to resolution.

- Pileup correction: 30 % of the size of pileup correction is quoted as the pileup correction systematic uncertainty. The pileup correction is obtained from the minimum bias data. The energy away from jets (electron) in dijet ($W \to e\nu$) events, and the photon-jet p_T balance in photon+jet events as a function of the number of reconstructed primary vertices were also measured. The systematic uncertainty is determined so that the quoted uncertainty covers variations from all of these cross-check studies. This uncertainty results in less than 3 % uncertainty in the cross section measurement.

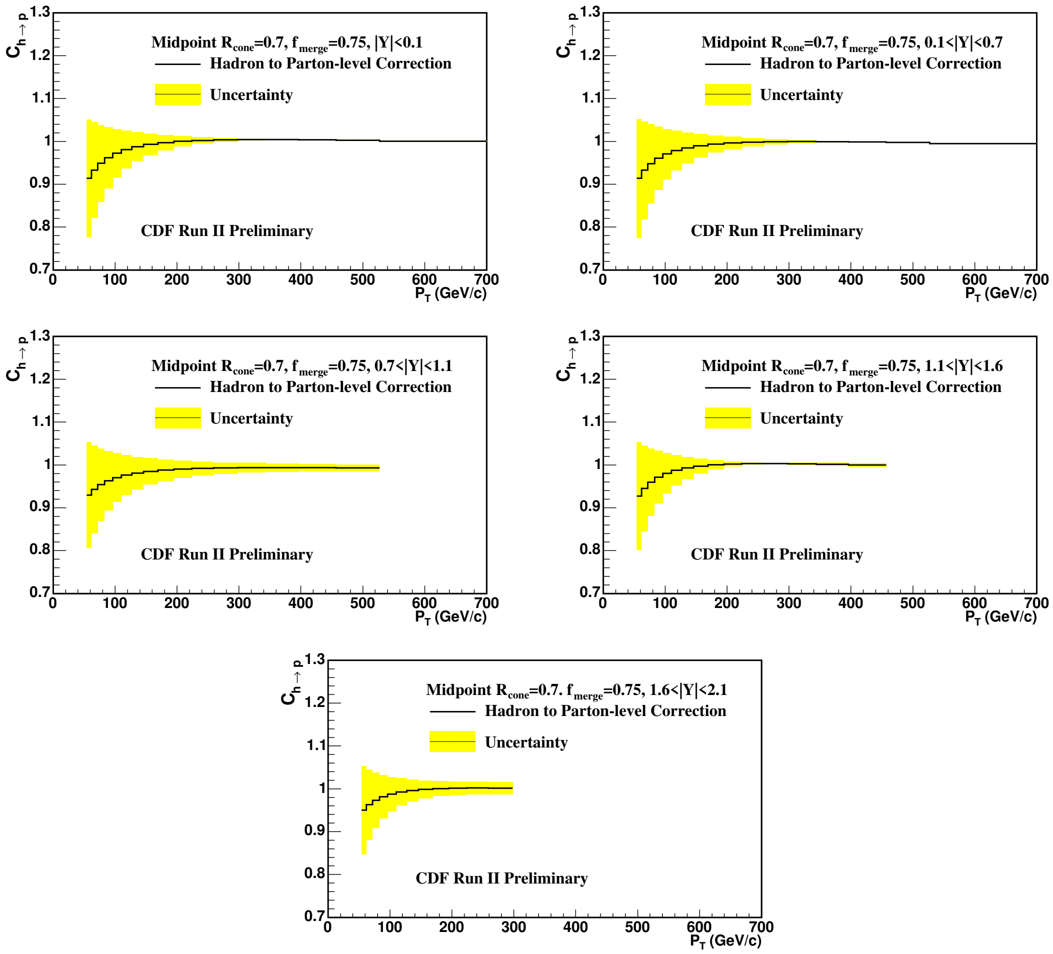

FIG. 3: The hadron to parton level correction applied is shown for each y region. The difference between the HERWIG and PYTHIA prediction for this correction is conservatively taken as the systematic uncertainty. The magnitude of the difference between the HERWIG and PYTHIA predictions is represented by the yellow shaded bands.

- Luminosity: 6 % uncertainty in normalization [23].
- Hadron-level to parton-level correction: The systematic uncertainty on the hadron to parton level correction is estimated from the difference in the predictions for this correction from HERWIG and PYTHIA. HERWIG does not include multiple parton interactions (MPI) in its UE model, and instead relies on initial state radiation (ISR) and beam remnants to populate the UE. PYTHIA includes MPI as well as the components included in HERWIG. PYTHIA therefore predicts a larger correction at low p_T where the ISR of HERWIG is too 'soft'. We conservatively take the difference between HERWIG and PYTHIA for this systematic uncertainty, and this systematic is represented by the yellow bands in figure 3.

VI. THEORETICAL PREDICTIONS

The prediction of pQCD was obtained from the next-to-leading order (NLO) program NLOJET++ [24–26] with CTEQ6.1M [2] parton distribution functions (PDFs). The μ scale was chosen as the transverse momentum of the jet divided by two, which is the same as that used to determine the PDF. Using $\mu = p_T^{jet}$ and $2 \times p_T^{jet}$ gives $\sim$ 10 and 20 % smaller predictions in the cross section. The value of 1.3 was used for R_{sep} which is used for the Midpoint algorithm at the parton level to mimic the splitting and merging step of the Midpoint algorithm when combining calorimeter towers, particles after hadronization, or partons after the parton shower [9]. A R_{sep} value of 2.0 (*i.e.,* the midpoint algorithm without R_{sep}) correspnds to a < 5 % larger prediction for the cross section at NLO.

VII. RESULTS

The results of the inclusive jet cross section measurement using 1.13 fb^{-1} of integrated luminosity are shown in figures 4- 8. In each figure the inclusive differential jet cross section corrected to the hadron level is shown on the left, and the ratio of data corrected to the parton level to the NLO predictions of NLOJET++ are shown on the right. The systematic uncertainty on the measurement corrected to the hadron level is shown in yellow, while the uncertainty due to the hadronization and underlying event correction is shown in blue. The PDF uncertainty is drawn in red on the ratio plots [27]. The cross sections for the various rapidity regions have been scaled on figure 9 for presentation purposes. Figure 10 includes the ratio to NLO pQCD predictions for all rapidity regions.

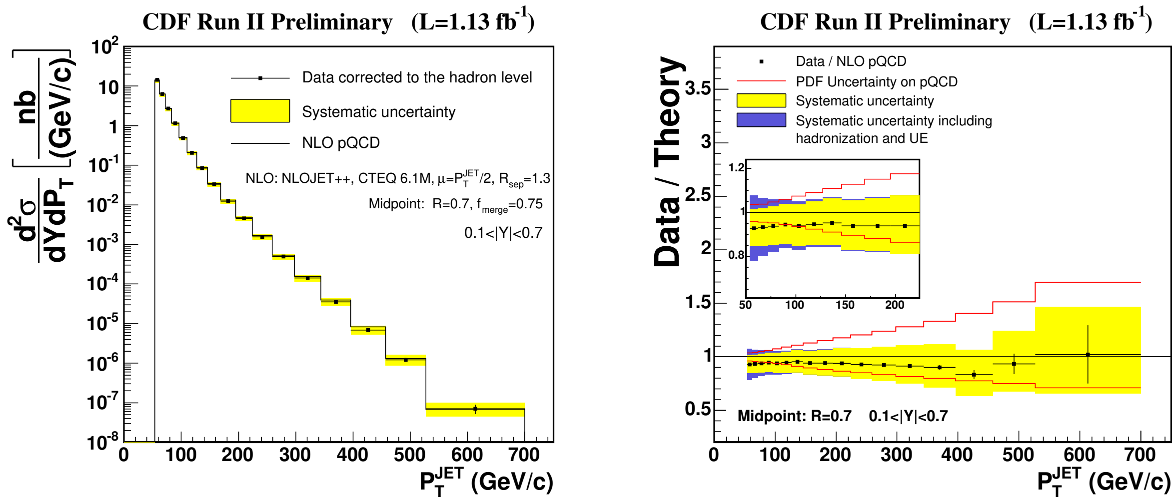

FIG. 4: Measured inclusive jet cross section with the Midpoint algorithm in the region $0.1 < |y| < 0.7$. The distribution for the hadron level cross section is shown on the left, while the ratio of data corrected to the parton level to the NLO pQCD prediction of NLOJET++ is shown on the right.

VIII. CONCLUSIONS

A measurement was presented of the inclusive jet cross section for jets clustered by the CDF midpoint jet finding algorithm using 1.13 fb^{-1} of data collected by the CDF experiment. Good agreement is seen in all rapidity regions with the pQCD predictions of the NLO program NLOJET++ using CTEQ6.1M parton distributions. In the forward region ($|y| > 1.6$) the systematic uncertainty on the measurement is smaller than the PDF uncertainty which suggests that this measurement will lead to useful constraints on global PDF fits.

Acknowledgments

We thank the Fermilab staff and the technical staffs of the participating institutions for their vital contributions. This work was supported by the U.S. Department of Energy and National Science Foundation; the Italian Istituto Nazionale di Fisica Nucleare; the Ministry of Education, Culture, Sports, Science and Technology of Japan; the Natural Sciences and Engineering Research Council of Canada; the National Science Council of the Republic of China; the Swiss National Science Foundation; the A.P. Sloan Foundation; the Bundesministerium fuer Bildung und Forschung, Germany; the Korean Science and Engineering Foundation and the Korean Research Foundation; the Particle Physics and Astronomy Research Council and the Royal Society, UK; the Russian Foundation for Basic Research; the Comision Interministerial de Ciencia y Tecnologia, Spain; and in part by the European Community's

Human Potential Programme under contract HPRN-CT-20002, and the Academy of Finland.

---

[1] E. Eichten, K. D. Lane, and M. E. Peskin, Phys. Rev. Lett. **50**, 811 (1983).
[2] D. Stump et al., JHEP **10**, 046 (2003), hep-ph/0303013.
[3] D. J. Gross and F. Wilczek, Phys. Rev. **D8**, 3633 (1973).
[4] H. Fritzsch, M. Gell-Mann, and H. Leutwyler, Phys. Lett. **B47**, 365 (1973).
[5] J. Huston et al., Phys. Rev. **D58**, 114034 (1998), hep-ph/9801444.
[6] A. A. Affolder et al. (CDF Collaboration), Phys. Rev. **D64**, 032001 (2001), hep-ph/0102074.
[7] A. Abulencia et al. (CDF Collaboration), Phys. Rev. **D74**, 071103 (2006), hep-ex/0512020.
[8] G. C. Blazey et al. (2000), hep-ex/0005012.
[9] S. D. Ellis, J. Huston, and M. Tonnesmann, eConf **C010630**, P513 (2001), hep-ph/0111434.
[10] A. Abulencia et al. (CDF Collaboration), Phys. Rev. Lett. **96**, 122001 (2006), hep-ex/0512062.
[11] A. Abulencia et al. (CDF Collaboration), Phys. Rev. **D75**, 092006 (2007), hep-ex/0701051.
[12] F. Abe et al. (CDF Collaboration), Nucl. Instr. Meth. **A271**, 387 (1988).
[13] P. T. Lukens (CDF Collaboration) (2003), fERMILAB-TM-2198.
[14] B. L. Winer, Int. J. Mod. Phys. **A16S1C**, 1169 (2001).
[15] T. Sjostrand et al., Comput. Phys. Commun. **135**, 238 (2001), hep-ph/0010017.
[16] G. Corcella et al., JHEP **01**, 010 (2001), hep-ph/0011363.
[17] H. L. Lai et al. (CTEQ), Eur. Phys. J. **C12**, 375 (2000), hep-ph/9903282.
[18] R. Brun, F. Bruyant, M. Maire, A. C. McPherson, and P. Zanarini (1987), cERN-DD/EE/84-1.
[19] G. Grindhammer, M. Rudowicz, and S. Peters, Nucl. Instrum. Meth. **A290**, 469 (1990).
[20] A. Bhatti et al. (2005), hep-ex/0510047.
[21] P. Bagnaia et al. (UA2), Phys. Lett. **B144**, 283 (1984).
[22] R. Field and R. C. Group (CDF Collaboration) (2005), hep-ph/0510198.
[23] D. Acosta et al., Nucl. Instrum. Meth. **A494**, 57 (2002).
[24] Z. Nagy, Phys. Rev. **D68**, 094002 (2003), hep-ph/0307268.
[25] S. Catani and M. H. Seymour, Nucl. Phys. **B485**, 291 (1997), hep-ph/9605323.
[26] T. Kluge, K. Rabbertz, and M. Wobisch (0900), hep-ph/0609285.
[27] J. Pumplin et al., Phys. Rev. **D65**, 014013 (2002), hep-ph/0101032.
[28] M. G. Albrow et al. (TeV4LHC QCD Working Group) (2006), hep-ph/0610012.
[29] We use a cylindrical coordinate system with the z coordinate along the proton beam direction and the origin at the center of the detector, the azimuthal angle ϕ, and the polar angle θ usually expressed through the pseudorapidity $\eta = -\ln\tan(\theta/2)$. The rapidity y is defined as $y = -1/2\ln((E+p_z)/(E-p_z))$ where E denotes the energy and P_Z is the momentum component along z. The transverse energy and transverse momentum are given by: $E_T = E\sin(\theta)$ $p_T = p\sin(\theta)$ where p is the magnitude of the momentum vector.
[30] In previous CDF studies an additional step called the "Search Cone" was included in the Midpoint algorithm. For a discussion of the Search Cone versus Midpoint see Ref [28].
[31] The missing transverse energy ($\vec{\not{E}}_T$) is defined by, $\vec{\not{E}}_T = -\sum_i E_T^i \hat{\mathbf{n}}_\mathbf{i}$, where $\hat{\mathbf{n}}_\mathbf{i}$ is a unit vector perpendicular to the beam axis and pointing at the ith calorimeter tower. Missing E_T significance is defined by, $\widetilde{\not{E}_T} = \not{E}_T/\sqrt{\sum E_T}$.
[32] The hadron level in the Monte Carlo generators is defined using all final-state particles with lifetime above 10^{-11}s.
[33] R. Field, presented at *Fermilab ME/MC Tuning Workshop*, Fermilab, October 4, 2002.
[34] PYTHIA-Tune A implies that the following parameters are set in PYTHIA (CTEQ5L): PARP(67)=4, MSTP(82)=4, PARP(82)=2, PARP(84)=0.4, PARP(85)=0.9, PARP(86)=0.95, PARP(89)=1800, PARP(90)=0.25.

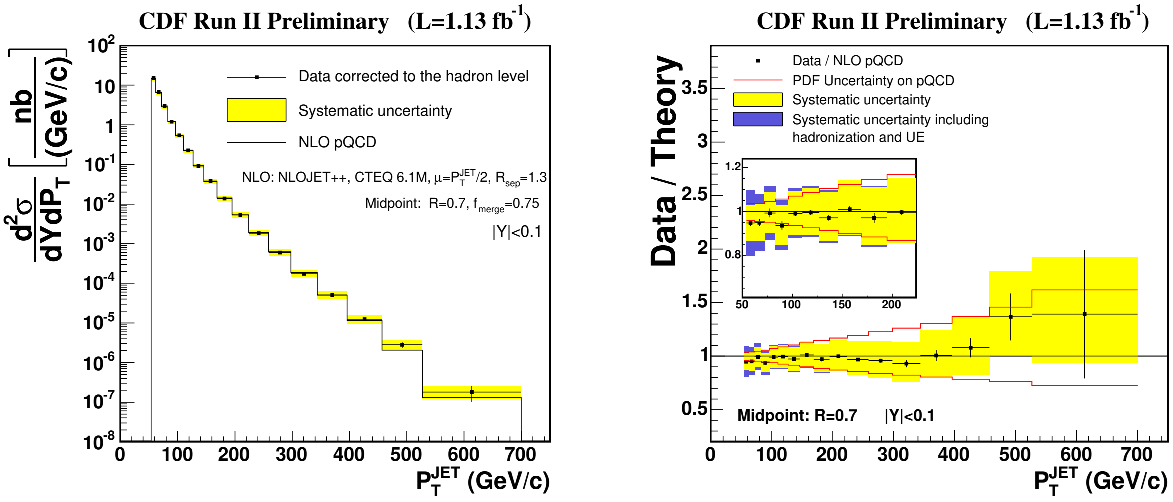

FIG. 5: Measured inclusive jet cross section with the Midpoint algorithm in the region $|y| < 0.1$. The distribution for the hadron level cross section is shown on the left, while the ratio of data corrected to the parton level to the NLO pQCD prediction of NLOJET++ is shown on the right.

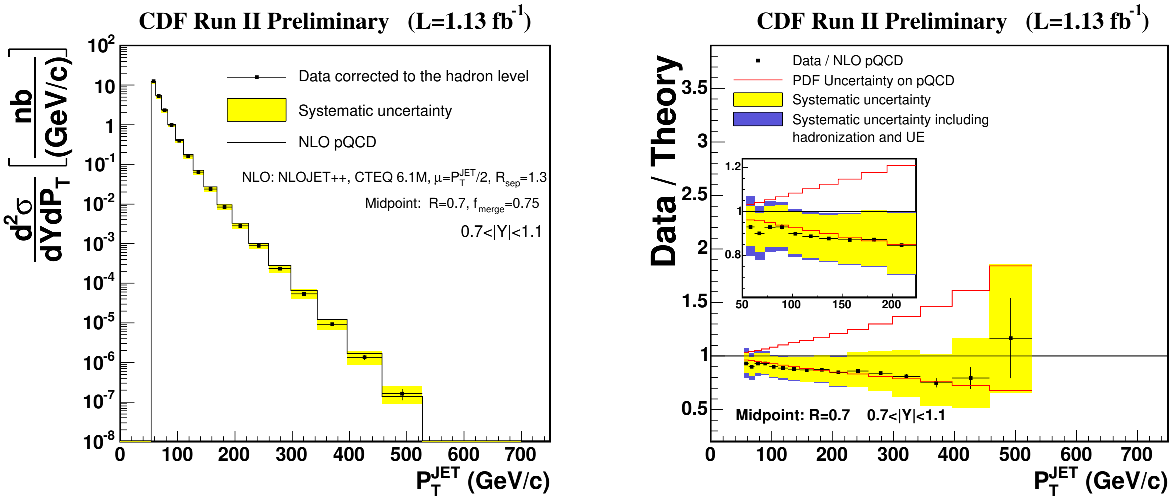

FIG. 6: Measured inclusive jet cross section with the Midpoint algorithm in the region $0.7 < |y| < 1.1$. The distribution for the hadron level cross section is shown on the left, while the ratio of data corrected to the parton level to the NLO pQCD prediction of NLOJET++ is shown on the right.

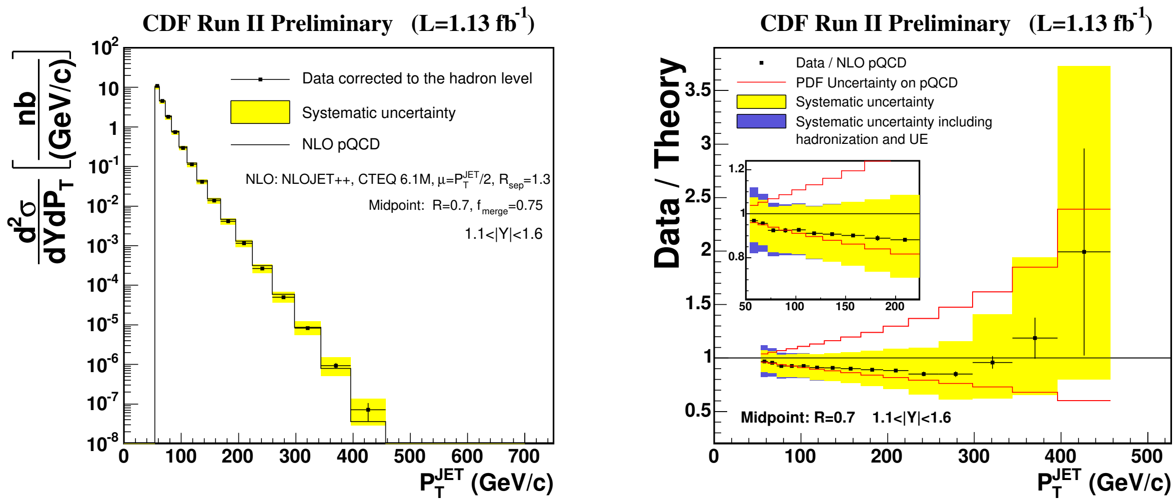

FIG. 7: Measured inclusive jet cross section with the Midpoint algorithm in the region $1.1 < |y| < 1.6$. The distribution for the hadron level cross section is shown on the left, while the ratio of data corrected to the parton level to the NLO pQCD prediction of NLOJET++ is shown on the right.

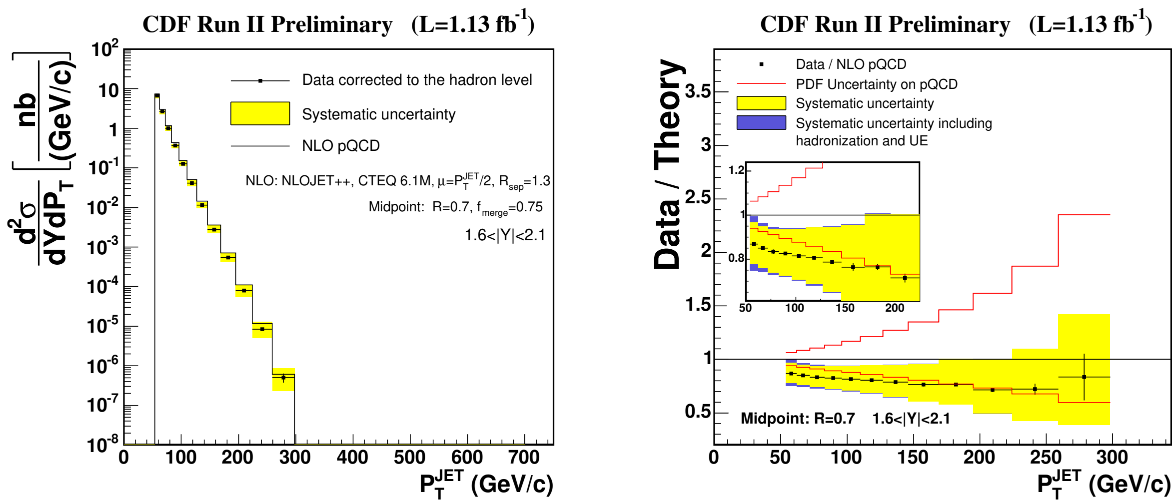

FIG. 8: Measured inclusive jet cross section with the Midpoint algorithm in the region $1.6 < |y| < 2.1$. The distribution for the hadron level cross section is shown on the left, while the ratio of data corrected to the parton level to the NLO pQCD prediction of NLOJET++ is shown on the right.

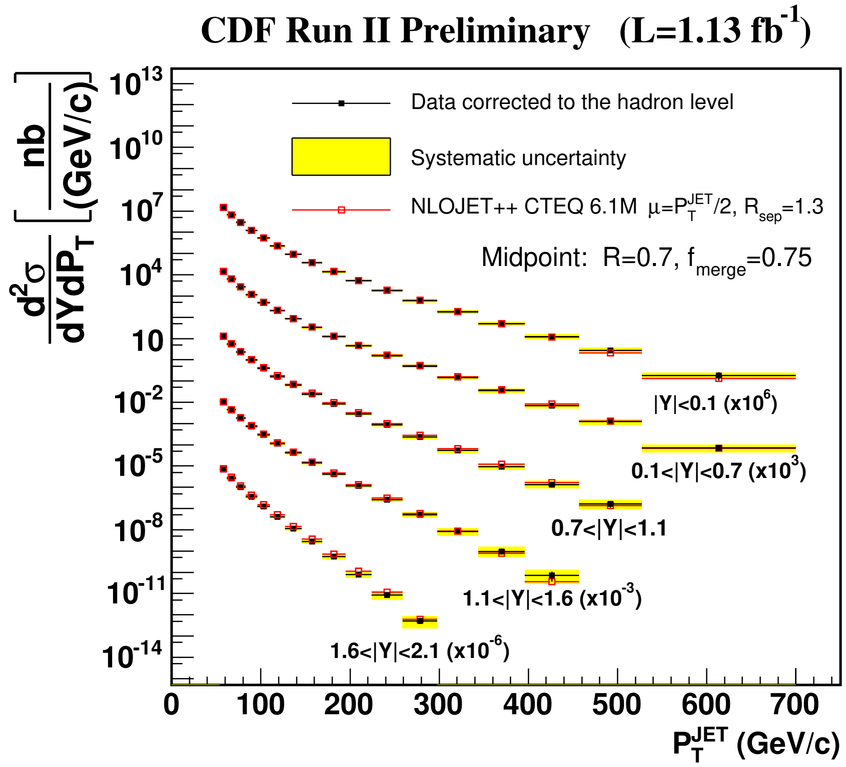

FIG. 9: Measured inclusive jet cross section at the hadron level with the Midpoint algorithm in all rapidity regions.

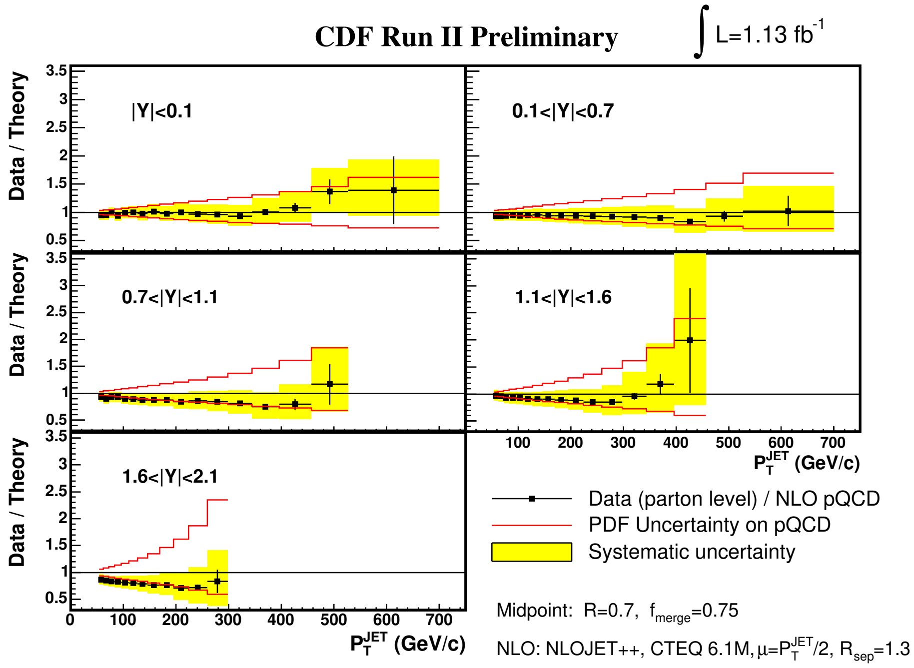

FIG. 10: The ratio of the measured inclusive jet cross section at the parton level with the Midpoint algorithm to the NLO pQCD prediction of NLOJET++ in five rapidity regions.